Title

Status of Lattice QCD Determination of Nucleon Form Factors and Their Relevance for the Few-GeV Neutrino Program

Journal

Annual Review of Nuclear and Particle Science, 72(1)

ISSN

0163-8998

Authors

Meyer, AS

Walker-Loud, A

Wilkinson, C

Publication Date

2022-09-26

DOI

10.1146/annurev-nucl-010622-120608

ANNUAL REVIEWS

Annual Review of Nuclear and Particle Science

Status of Lattice QCD Determination of Nucleon Form Factors and Their Relevance for the Few-GeV Neutrino Program

Aaron S. Meyer,[1,2] André Walker-Loud,[2] and Callum Wilkinson[3]

[1]Department of Physics, University of California, Berkeley, California, USA; email: asmeyer@berkeley.edu

[2]Nuclear Science Division, Lawrence Berkeley National Laboratory, Berkeley, California, USA

[3]Physics Division, Lawrence Berkeley National Laboratory, Berkeley, California, USA

Annu. Rev. Nucl. Part. Sci. 2022. 72:205–32

First published as a Review in Advance on July 8, 2022

The *Annual Review of Nuclear and Particle Science* is online at nucl.annualreviews.org

https://doi.org/10.1146/annurev-nucl-010622-120608

Keywords

neutrino oscillations, nucleon form factors, lattice QCD

Abstract

Calculations of neutrino–nucleus cross sections begin with the neutrino–nucleon interaction, making the latter critically important to flagship neutrino oscillation experiments despite limited measurements with poor statistics. Alternatively, lattice quantum chromodynamics (LQCD) can be used to determine these interactions from the Standard Model with quantifiable theoretical uncertainties. Recent LQCD results of g_A are in excellent agreement with data, and results for the (quasi-)elastic nucleon form factors with full uncertainty budgets are expected within a few years. We review the status of the field and LQCD results for the nucleon axial form factor, $F_A(Q^2)$, a major source of uncertainty in modeling sub-GeV neutrino–nucleon interactions. Results from different LQCD calculations are consistent but collectively disagree with existing models, with potential implications for current and future neutrino oscillation experiments. We describe a road map to solidify confidence in the LQCD results and discuss future calculations of more complicated processes, which are important to few-GeV neutrino oscillation experiments.

Contents

1. INTRODUCTION

A major experimental program is underway that seeks to measure as-of-yet unknown properties associated with the change of flavor of neutrinos. In particular, the neutrino mass hierarchy and charge parity (*CP*)-violating phase of neutrinos still remain to be measured, with additional focuses on measuring oscillation parameters with high precision and testing whether the current three-flavor mixing paradigm is sufficient (1, 2). These goals introduce stringent requirements on the precision of current and future experiments. High-intensity beams are required to produce a sufficient flux of neutrinos to accumulate the necessary statistics. Increased statistics place additional burden on our understanding of the systematic uncertainties needed for the experimental program.

Two large-scale, next-generation experiments designed to meet these experimental constraints are the Deep Underground Neutrino Experiment (DUNE) (3) and Hyper-Kamiokande (Hyper-K) (4). DUNE has a broad neutrino energy spectrum with a peak at a neutrino energy of ∼2.5 GeV, with significant contributions between 0.1 and 10 GeV, over a 1,295-km baseline. Hyper-K has a narrow neutrino energy spectrum that peaks at a neutrino energy of ∼0.6 GeV, with significant contributions between 0.1 and 2 GeV, over a 295-km baseline. Despite their different energies (E) and baselines (L), both experiments sit at a similar energy-to-baseline ratio and therefore probe similar oscillation physics. At the few-GeV energies of interest, neutrino–nucleon (νN) interactions have many available interaction channels, including quasielastic, resonant, and deep inelastic scattering (5–9).

Theoretical models that make different physical assumptions are typically used to model each interaction channel, with ad hoc interpolations to fill in gaps between the models. Additionally, all current and planned experiments use target materials predominantly composed of hydrocarbons, liquid argon, or water, in which the nucleons are not free. The selection of such materials avoids serious experimental complications associated with using elementary targets (e.g., liquid hydrogen) and increases the interaction rate in a given detector volume owing to their higher densities. However, the presence of multiple interaction channels and the addition of nuclear effects significantly complicate the analysis of data from neutrino experiments and give rise to a major source of systematic uncertainty: Intranuclear motion can be significant relative to the energy transfer for the interactions of interest; interactions with correlated nucleon–nucleon states can modify or redistribute the interaction strength; rescattering of pions and nucleons in the nucleus can confuse the relationship between the particles associated with the primary interaction channels and

those observed in the detector; and rescattering can manifest as changes to the particle content and changes to the fraction of energy lost to neutrons, which are typically unobservable in the detectors used by few-GeV neutrino oscillation experiments.

A significant challenge impeding progress toward a consistent theoretical description of νA scattering is the lack of data with which to benchmark parts of the calculation. For example, neutrino quasielastic scattering ($\nu_l + n \to l^- + p$ or $\bar{\nu}_l + p \to l^+ + n$) is the simplest of the relevant hard scattering processes and dominates the neutrino cross section below energies of ∼1 GeV. However, modern experiments using nuclear targets are unable to measure it without significant nuclear effects (9, 10). Instead, they select a specific interaction topology, such as one muon and no pions, that will be dominated by quasielastic processes. This event selection will still have significant contributions from resonant pion production events where the pion has rescattered in the nucleus and has either been absorbed or has lost sufficient energy to be below the detection threshold. Given the challenge to benchmark neutrino cross-section models for quasielastic scattering (and other hard scattering processes) with new νA data sets, experimentalists and theorists have relied heavily on sparse data from the 1960s–1980s from several bubble-chamber experiments that used H_2 or D_2 targets (2, 5). The small neutrino cross section and relatively weak (by modern standards) accelerator neutrino beams used by these early experiments mean that the available quasielastic event sample on light targets amounts to a few thousand events (11–15).[1] These data do not have sufficient power to constrain theoretical models satisfactorily (18, 19). As a result, there is insufficient information about fundamental νN scattering processes on which to build a complete model for neutrino–nucleus (νA) scattering, a substantial limitation that has serious implications for the precision goals of future experiments.

Experimentalists are looking for other ways to access neutrino interactions with elementary targets for the purpose of disambiguating neutrino cross-section modeling uncertainties. Safety considerations make it unlikely that new high-statistics bubble-chamber experiments using hydrogen or deuterium will be deployed to fill this crucial gap. An alternative possibility is to use various hydrocarbon targets to subtract the carbon interaction contributions from the total hydrocarbon event rates and produce "on-hydrogen" measurements (20–24). Although these ideas are promising, they typically rely on kinematic tricks that are relevant only for some channels, and it remains to be seen whether the systematic uncertainty associated with modeling the carbon subtraction can be adequately controlled. Such ideas may also be extended to other compound target materials with hydrogen or deuterium components.

Lattice quantum chromodynamics (LQCD) can be used to determine the free nucleon amplitudes that are otherwise not known at the required precision without the need for another experiment. LQCD provides a theoretical method for predicting the free nucleon amplitudes directly from the Standard Model of particle physics with systematically improvable theoretical uncertainties. Recently, an LQCD milestone was achieved when the nucleon axial coupling[2] was determined with a 1% total uncertainty and a value consistent with experiment (25). LQCD can also provide percent- to few-percent-level uncertainties for the nucleon quasielastic axial form factor with momentum transfers up to a few GeV^2. Similarly, current tension in the neutron magnetic form factor parameterization, which is roughly half the size of the total axial form factor

LQCD: lattice quantum chromodynamics

Axial coupling: the axial form factor at zero momentum transfer, $g_A = F_A(0)$

[1]Some constraints on the axial form factor have been obtained from fits to electro pion production data. The fits are parameterized by a low energy theory that is valid in the chiral ($m_\pi \to 0$) limit and at small three-momentum and energy transfer, with model-dependent systematics that are significant and not typically quantified. These data will not be considered in this review. For more details, we refer the reader to References 16 and 17.

[2]Within the LQCD community, the axial coupling is commonly referred to as the axial charge.

uncertainty, can be resolved with LQCD calculations. Such results are anticipated in the next year or so with computing power available in the present near-exascale computing era.

Building upon these critical quantities, more challenging computations can provide information about nucleon resonant and nonresonant contributions to vector and axial-vector matrix elements, such as the Δ and Roper resonance channels, pion production, inclusive contributions in the shallow inelastic scattering region, and deep inelastic scattering parton distribution functions. Additionally, LQCD calculations of two-nucleon response functions would provide crucial information for our theoretical understanding of important two-body currents that are needed for building νA cross sections from νN amplitudes.

Given the present state of the field, in this review we focus on elastic single-nucleon amplitudes, for which we anticipate the LQCD results will produce impactful results for experimental programs in the next year or two. We begin in Section 2 by surveying the existing status and tensions in the field for the single-nucleon (quasi-)elastic form factors. Then, in Section 3, after providing a high-level introduction to LQCD, we survey existing results of the axial form factor. This includes the role of the partially conserved axial current (PCAC) relation in the calculations as well as use of the z expansion for combining the continuum and physical pion mass extrapolations. In Section 4, we discuss the potential impact of using LQCD determinations of the axial form factor when modeling νA cross sections. In Section 5, we comment on the most important improvements to be made in LQCD calculations, and we conclude in Section 6.

PCAC: partially conserved axial current

CCQE: charged-current quasielastic

dipole parameterization: $F_D(Q^2) \equiv (1 + Q^2/M_D^2)^{-2}$

BBBA05: the Bradford-Bodek-Budd-Arrington 2005 nucleon elastic form factor parameterization

2. STATUS OF SINGLE-NUCLEON (QUASI-)ELASTIC FORM FACTORS

For charged-current quasielastic (CCQE) νN scattering, the neutron ($|n\rangle$) to proton ($\langle p|$) interaction is mediated by a $V-A$ weak current, given at the quark level by $\bar{u}\gamma_\mu(1-\gamma_5)d$ (or its conjugate for proton to neutron). The nucleon-level amplitude at four-momentum transfer $Q^2 = -q^2$ is parameterized by

$$\langle p|V^\mu|n\rangle = \bar{U}_p(p+q)\Big[F_1^+(q^2)\gamma^\mu + \frac{i}{2M}F_2^+(q^2)\sigma^{\mu\nu}q_\nu\Big]U_n(p),$$
$$\langle p|A^\mu|n\rangle = \bar{U}_p(p+q)\Big[F_A^+(q^2)\gamma^\mu\gamma_5 + \frac{1}{M}F_P^+(q^2)q^\mu\gamma_5\Big]U_n(p). \quad 1.$$

The isovector form factors F_1^+ and F_2^+ can be precisely estimated from electron–nucleon scattering data. Electron–proton and electron–neutron scattering are sensitive to linear combinations of the isoscalar ($F_{1,2}^s$) and isovector ($F_{1,2}^3$) form factors. After isolating $F_{1,2}^3$, approximate isospin symmetry can be used to relate these τ_3 form factors to the charged τ_+ form factors of Equation 1: In the isospin limit, $\langle p|\bar{u}\,\Gamma u - \bar{d}\,\Gamma d|p\rangle = \langle p|\bar{u}\,\Gamma d|n\rangle$ for Dirac structure Γ, and $F_{1,2}^3 = F_{1,2}^+$ for the isovector Dirac and Pauli form factors.

However, there is a significant tension in existing parameterizations of the proton magnetic form factor extracted from those data, as shown in **Figure 1**. Two different parameterizations of the form factor, normalized by a dipole parameterization, are shown: the BBBA05 (26) parameterization and a more recent z expansion parameterization from Borah et al. (27). The tension is significant over all $Q^2 > 0$, at the level of several percent, including significant disagreement in the slope of the form factor at $Q^2 = 0$. LQCD computations of the vector form factors are also the most mature of the nucleon matrix elements, exhibiting no obvious tensions with experimental determinations at their current level of precision. A percent-level calculation of the form factor Q^2 behavior or a direct calculation of the magnetic form factor slope could potentially discriminate between the two parameterizations.

The axial coupling is a key benchmark for LQCD and is precisely known from neutron decay experiments (28). LQCD calculations of the axial coupling have historically been low compared

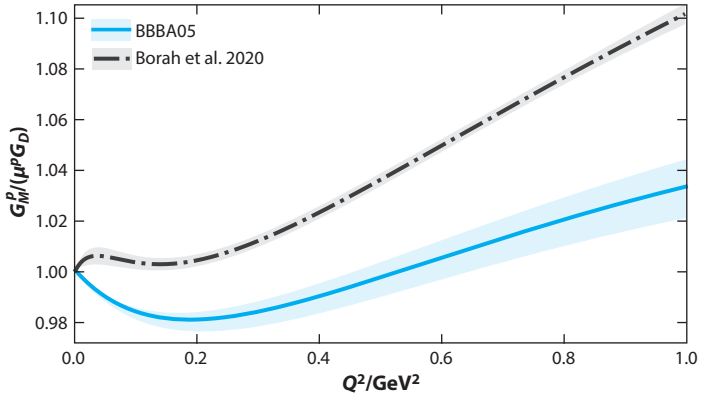

Figure 1

Proton magnetic form factor normalized by a reference dipole ansatz with a dipole mass of 0.84 GeV. The gray band indicates the proton-only fit to a z expansion by Borah et al. (27) (the *dashed black line* indicates the mean value). The blue band indicates the BBBA05 parameterization (26) (the *solid blue line* indicates the mean value). Figure adapted from Reference 27 (figure 4 and associated supplemental data; CC BY 4.0).

with experiment (29), and the discrepancy has been the topic of some controversy. It is now understood that the treatment of excited-state systematics is the main culprit for this discrepancy (29–31). This topic, and how it pertains to the full momentum dependence of the form factor, is discussed in detail in Section 3.3. With proper control over the excited-state contamination, LQCD calculations are now in good agreement with the experimental value (32–43); one group has achieved a subpercent determination of g_A (25, 44, 45).

The success in calculating the threshold value g_A motivates current efforts to map out $F_A(Q^2)$, which is of importance to the long-baseline neutrino program. The need for this is clear: Sparse data from deuterium bubble-chamber experiments do not constrain the axial form factor precisely. The popular dipole ansatz has a shape that is overconstrained by data, resulting in an underestimated uncertainty. Employing a model-independent z expansion parameterization relaxes the strict shape requirements of the dipole and yields a more realistic uncertainty that is nearly an order of magnitude larger (18). The axial radius, which is proportional to the slope of the form factor at $Q^2 = 0$, has a 50% uncertainty when estimated from the deuterium scattering data, or ∼35% if deuterium scattering and muonic hydrogen are considered together (19). Given that a modern νN scattering experiment is extremely unlikely, LQCD is the only viable method to improve our understanding of the axial form factor to the required level of precision.

A striking feature of LQCD calculations of $F_A(Q^2)$ is the slower falloff (compared with what is extracted from experiment) with increasing Q^2 (Section 3.4). This preference is consistently reproduced by several lattice collaborations using independent computation methods, lending more credence to the result. The nucleon cross section is obtained by integrating over Q^2, and the slower falloff with Q^2 translates to an enhancement by as much as 30–40% for neutrino energies greater than 1 GeV (Section 4). In addition, the precision of the axial form factor uncertainty from LQCD is small enough to be sensitive to the tension between vector form factor parameterizations. The aforementioned situation with nucleon form factors is depicted in **Figure 2**.

3. LQCD DETERMINATIONS OF NUCLEON FORM FACTORS

LQCD has been and remains one of the major uses of the world's Leadership Computing Facilities. There is an extensive literature on LQCD that covers the broad range of technical and

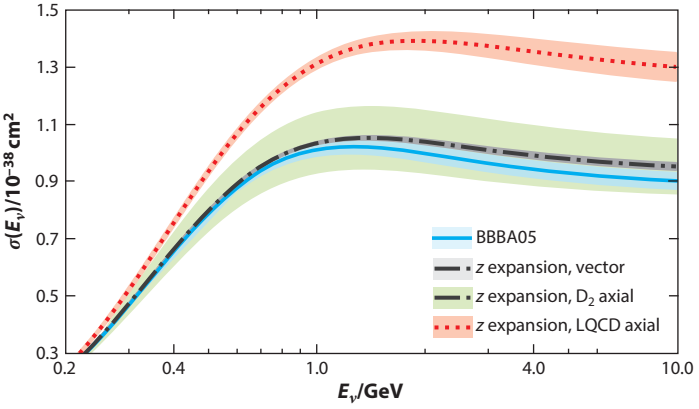

Figure 2

Neutrino cross sections on a free neutron, with their uncertainty bands, for various choices of parameterization. For BBBA05, the vector form factors are from Bradford et al. (i.e., BBBA05; 26), and the axial form factors are from Meyer et al. (18). The uncertainty is taken only from the BBBA05 parameterization, and all fit parameters are assumed to be uncorrelated. For the z expansion–vector parameterization, the vector form factors are from Borah et al. (27), and the axial form factors are from Meyer et al. (18). The uncertainty is taken only from Borah et al. (27). The z expansion–D_2 axial parameterization is the same as the z expansion–vector parameterization, except the uncertainty is instead taken only from Meyer et al. (18). For the z expansion–LQCD axial parameterization, the vector form factors are from Borah et al. (27), and the axial form factor with its uncertainty is from an LQCD simulation on a single physical mass ensemble (111). Of particular note is the observed tension between the black and blue bands, which results from the tension between proton magnetic form factor parameterizations (see **Figure 1**). The width of the upper red band, which comes from the LQCD results, is comparable in size to the discrepancy between these black and blue curves. The LQCD uncertainty is also noticeably smaller than the green band that arises from the deuterium scattering determination of $F_A(Q^2)$. The normalization of the red curve is higher because of the slower falloff of the axial form factor. Abbreviation: LQCD, lattice quantum chromodynamics.

formal aspects necessary to carry out state-of-the-art calculations, for which we cannot do justice in this review. For an in-depth introduction to LQCD, we refer readers to a few standard textbooks (46–48). In this review, we provide a high-level summary of general issues that must be addressed as well as issues specific to LQCD calculations of nucleon matrix elements and form factors. These issues are also discussed in detail in the biannual Flavour Lattice Averaging Group (FLAG) reviews [see, e.g., the most recent one (29)].

The promise of LQCD is to provide Standard Model predictions of low-energy hadronic and nuclear quantities with fully quantified theoretical uncertainties. To achieve this goal, several sources of systematic uncertainty must be assessed. These include extrapolations to the continuum and infinite-volume limits as well as an extrapolation or interpolation to the physical quark mass limit. At least three values of the lattice spacing, a, of O($a \lesssim 0.12$ fm) are required to ascertain whether the leading discretization corrections are sufficient to describe the observed scaling violations (do all three results lie on a straight line, or can one detect higher-order curvature?). For the finite-volume effects, a rule of thumb has been established from experience: Calculations with $m_\pi L \gtrsim 4$ (where L is the spatial extent of the lattice volume) are required so that these finite-sized corrections remain at the level of $\lesssim$1–2% and can be at least qualitatively described by the leading analytic formulae.

For the light quark mass dependence, chiral perturbation theory (χPT) may be able to guide the extrapolations. However, for the nucleon, the convergence of χPT is not yet established, even

FLAG: Flavour Lattice Averaging Group

Chiral perturbation theory (χPT): the low-energy effective field theory of QCD

at the physical pion mass, with an evident lack of convergence for the nucleon mass and g_A (25, 45). As we discuss further in Section 3.2, there are two additional significant sources of uncertainty for nucleons: the exponentially degrading signal-to-noise (S/N) problem and excited-state contamination.

S/N: signal-to-noise

HMC: Hybrid Monte Carlo

Configuration: a sample of the gluon field; a set of configurations all generated with the same bare QCD parameters is called an ensemble

Universality: all valid choices of discretized QCD become QCD as $a \to 0$

EFT: effective field theory

3.1. LQCD: A High-Level Summary

The QCD path integral is quadratic in the quark fields, allowing for an analytic integration over the fermionic fields. In Euclidean space, one has the gluonic integral

$$Z_{\mathrm{QCD}} = \int DU \, \mathrm{Det}[\not{D}(U) + m_q] \, e^{-S_{\mathrm{G}}(U)}, \qquad 2.$$

with gluon action $S_{\mathrm{G}}(U)$ and the determinant of the quark operator $\mathrm{Det}[\not{D}(U) + m_q]$, for each flavor of quark simulated. Even at finite lattice spacing and volume, the multidimensional integral is vastly too large to perform. However, in Euclidean space, both S_{G} and the fermion determinant are real and positive for zero chemical potential, and so the integral can be approximated with a hybrid Monte Carlo (HMC) algorithm (49) using the factor $\mathrm{Det}[\not{D}(U) + m_q] \, e^{-S_{\mathrm{G}}(U)}$ as the importance sampling weight. In this way, a large number of configurations of gauge fields can be generated, providing a stochastic determination of the correlation functions

$$\langle O \rangle = \frac{1}{N_{\mathrm{cfg}}} \sum_{i=1}^{N_{\mathrm{cfg}}} O[U_i] + \mathrm{O}\left(\frac{1}{\sqrt{N_{\mathrm{cfg}}}}\right), \qquad 3.$$

where $O[U_i]$ is the correlation function evaluated on configuration i. The most expensive part of generating the configurations is evaluating the fermion determinant for the light and strange quarks. This is done with the use of pseudofermions (bosonic fields, ϕ)

$$Z_\psi = \int D\bar{\psi} D\psi \, e^{-\bar{\psi}[\not{D}(U)+m_q]\psi} = \mathrm{Det}[\not{D}(U) + m_q] = \int D\phi^\dagger D\phi \, e^{-\phi^\dagger \frac{1}{\not{D}(U)+m_q}\phi}, \qquad 4.$$

for which the bilinear operator is the inverse of the Dirac operator, which is a large, sparse matrix. Most of the algorithmic development for accelerating LQCD has gone into efficiently solving these large sparse matrices with large condition numbers. In particular, this is a problem very well suited for graphical processing units (GPUs) for which we have an advanced library, QUDA (50, 51; see also **https://github.com/lattice/quda**), developed for the international community.

There are many valid choices one can make in constructing the discretized lattice action, provided continuum QCD is recovered as $a \to 0$. This is known as the universality of the continuum limit, with each choice varying only at finite lattice spacing. Deviations from QCD, which arise at finite a, are often called discretization corrections or scaling violations. Universality is a property that can be proved in perturbation theory but must be established numerically given the nonperturbative nature of QCD. For sufficiently small lattice spacings, one can use effective field theory (EFT) to construct a continuum theory that encodes the discretization effects in a tower of higher-dimensional operators. This is known as the Symanzik EFT for lattice actions (52, 53). One interesting example involves the violation of Lorentz symmetry at finite lattice spacing: In the Symanzik EFT, the operators that encode Lorentz violation scale as a^2 with respect to the operators that survive the continuum limit. Thus, Lorentz symmetry is an accidental symmetry of the continuum limit. It is not respected at any finite lattice spacing, but the measurable consequences vanish as a^2 for sufficiently small lattice spacing.

As a concrete example of the Symanzik EFT, consider the discretized gluon action. The link fields are Wilson lines

$$U_\mu(x) = \exp\left\{ia \int_0^1 \mathrm{d}t A_\mu[x + (1-t)a\hat{\mu}]\right\} \approx \exp\left\{ia\bar{A}_\mu(x)\right\}. \qquad 5.$$

The gluon field $A_\mu(x)$ can be approximated as constant over the interval $[x, x + a\hat{\mu}]$, as expressed by $\bar{A}_\mu(x)$, with a being the lattice spacing. This parameterization allows for the construction of a discretized theory that preserves gauge invariance (54), a key property of gauge theories. In the continuum, the gluon action density is given by the product of field strength tensors, which are gauge-covariant curls of the gauge potential. When constructing the discretized gluon action, it is therefore natural to use objects that encode this curl of the gauge potential. The simplest such object is referred to as a plaquette and is given by

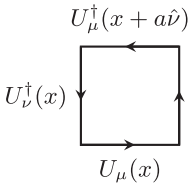

$$= U_{\mu\nu}(x) = U_\mu(x)U_\nu(x + a\hat{\mu})U_\mu^\dagger(x + a\hat{\nu})U_\nu^\dagger(x). \qquad 6.$$

For small lattice spacing, this Wilson gauge action reduces to the continuum action plus irrelevant (higher-dimensional) operators[3] that vanish in the continuum limit:

$$\begin{aligned} S_G(U) &= \beta \sum_{n=x/a} \sum_{\mu<\nu} \mathrm{Re}\left[1 - \frac{1}{N_c}\mathrm{Tr}\left[U_{\mu\nu}(n)\right]\right] \\ &= \frac{\beta}{2N_c} a^4 \sum_{n=x/a,\mu,\nu} \left[\frac{1}{2}\mathrm{Tr}\left[G_{\mu\nu}(n)G_{\mu\nu}(n)\right] + \mathrm{O}(a^2)\right], \qquad \rightarrow \beta = \frac{2N_c}{g^2}. \end{aligned} \qquad 7.$$

The continuum limit, which is the asymptotically large Q^2 region, is therefore approached as $\beta \rightarrow \infty$ where $g(Q^2) \rightarrow 0$.

The inclusion of quark fields adds more variety of lattice actions, each with its own benefits and drawbacks. There are four commonly used fermion discretization schemes: staggered fermions (55–58), clover-Wilson fermions (59), twisted mass fermions (60), and domain wall fermions (DWFs) (61–63). In this review, we make the following comments.

- Staggered fermions are the least expensive to simulate numerically, have leading scaling violations of $\mathrm{O}(a^2)$, and have a remnant chiral symmetry protecting the quark mass from additive mass renormalization. However, they split the four components of the fermion spinor onto different components of a local hypercube, mixing the Dirac algebra with space-time translations. This significantly complicates their use for baryons (64–66).
- Clover-Wilson fermions are the most commonly used discretization scheme given their theoretical simplicity and preservation of all symmetries except chiral symmetry. The explicit breaking of chiral symmetry with the Wilson operator means the light quark masses must be finely tuned against ultraviolet chiral symmetry breaking that scales as $1/a$, after which there remain residual $\mathrm{O}(a)$ chiral symmetry–breaking effects. It is well known, albeit laborious, how to nonperturbatively remove these leading $\mathrm{O}(a)$ scaling violations (67–70), which must be done for both the action and matrix elements.
- Twisted mass fermions are variants of Wilson fermions that exploit the approximate $SU(2)$ chiral symmetry of QCD to introduce a twisted quark mass term, $i\mu\gamma_5\tau_3$. This term is used to automatically remove the leading $\mathrm{O}(a)$ discretization effects (71), a benefit generically

[3] In the renormalization sense, irrelevant operators are operators of mass dimension $[O] > 4$, such that their dimensionful couplings scale as $a^n = \Lambda^{-n}$, where Λ is a high-energy scale that goes to infinity in the continuum limit for LQCD, and $n = [O] - 4$.

referred to as O(a) improvement, at the expense of introducing isospin breaking at finite lattice spacing.

- The fourth most common discretization is DWFs, which introduce a fifth dimension to the theory with unit links (the gluons are not dynamic in the fifth dimension) with the left- and right-handed fermions bound to opposite sides of the fifth dimension of size L_5. The overlap of these left and right modes gives rise to an explicit chiral symmetry breaking that is exponentially suppressed by the extent of the fifth dimension. For sufficiently small chiral symmetry breaking (large L_5), DWFs are also automatically O(a) improved. While very desirable, DWFs are more expensive to simulate numerically, both because of the extra fifth dimension and because of the algorithmic speedup offered by multigrid computational technique, which works tremendously for clover-Wilson fermions on GPUs (72) but is not yet fleshed out for DWF (73–77).
- A final common variant of action is one in which the fermion discretization used in the generation of the gauge fields (the sea quarks) and the action used when generating quark propagators (the valence quarks) are different; this is known as a mixed action (78). The most common reason to use such an action is to take advantage of numerically less expensive methods to generate the configurations while retaining good chiral symmetry properties of the valence quarks, which are known to suppress chiral symmetry–breaking effects from the sea quarks (79–82).

As mentioned above, a key assumption of LQCD is that all varieties of lattice action, for sufficiently small lattice spacing, are approximated by continuum QCD plus irrelevant operators whose contributions vanish in the continuum limit. It is important for the field to test this assumption of universality by computing the same quantities with a variety of lattice actions, at the level of both gluons and fermions, to gain confidence in the results that are extrapolated to the physical point.

3.2. Anatomy of LQCD Calculations of Nucleon Form Factors

Hadron masses are determined from LQCD by constructing two-point correlation functions in a mixed time–momentum representation. A common strategy uses spatially local creation operators (sources) and momentum space annihilation operators (sinks), taking advantage of momentum conservation to select the source momentum. The nonperturbative nature of QCD means we do not know how to construct the nucleon wave function, and so we use interpolating operators that have the quantum numbers of the state we are interested in. These creation and annihilation operators will couple to all eigenstates of QCD with the same quantum numbers, giving rise to a two-point function with a spectral decomposition:

$$C(t,\mathbf{p}) = \sum_{\mathbf{x}} e^{-i\mathbf{p}\cdot\mathbf{x}} \langle \Omega | O(t,\mathbf{x}) O^{\dagger}(0,\mathbf{0}) | \Omega \rangle = \sum_{n=0}^{\infty} z_n(\mathbf{p}) z_n^{\dagger}(\mathbf{p}) e^{-E_n(\mathbf{p})t}. \quad 8.$$

In this expression, $|\Omega\rangle$ is the vacuum state, $z_n(\mathbf{p}) = \sum_{\mathbf{x}} e^{-i\mathbf{p}\cdot\mathbf{x}} \langle \Omega | O(0,\mathbf{x}) | n \rangle$, and $z_n^{\dagger}(\mathbf{p}) = \langle n(\mathbf{p}) | O^{\dagger}(0,\mathbf{0}) | \Omega \rangle$. To go from the first equality to the second, we have inserted a complete set of states, $1 = \sum_n |n\rangle\langle n|$, and we have used the time-evolution operator to shift the annihilation operator to $t = 0$ and expose the explicit time dependence.[4] As we discuss in more detail below, it is more desirable to instead build both source and sink operators in momentum space. Momentum space sources are not commonly used because they are significantly more numerically expensive to generate.

[4]The Hamiltonian, $\hat{H}$, is used to time evolve the operator $O(t,\mathbf{x}) = e^{\hat{H}t} O(0,\mathbf{x}) e^{-\hat{H}t}$.

For large Euclidean time, the correlation function will be dominated by the ground state as the excited states will be exponentially suppressed by the energy gap:

$$C(t) = z_0 z_0^\dagger e^{-E_0 t}\left[1 + r_1 r_1^\dagger e^{-\Delta_{1,0} t} + \cdots\right], \quad \Delta_{m,n} = E_m - E_n, \quad r_n = \frac{z_n}{z_0}. \tag{9.}$$

It is useful to construct an effective mass to visualize at which time t the ground state begins to saturate the correlation function

$$m_{\text{eff}}(t) = \ln\left(\frac{C(t)}{C(t+1)}\right) = E_0 + \ln\left(1 + \sum_{n=1} r_n r_n^\dagger e^{-\Delta_{n,0} t}\right). \tag{10.}$$

For nucleon two-point functions, the S/N ratio degrades exponentially at large Euclidean time (83):

$$\lim_{\text{large } t} \text{S/N} \propto \sqrt{N_{\text{sample}}} e^{-(m_{\text{N}} - \frac{3}{2} m_\pi) t}. \tag{11.}$$

In the region in time when the ground state begins to saturate the correlation functions, typically around $t \approx 1$ fm, the noise becomes significant, which makes the correlation functions in this region susceptible to correlated fluctuations that can bias a simplistic single-state analysis. This forces measurements to be made at Euclidean times where excited-state contamination is still appreciable, which adds an extra source of systematic uncertainty. As the pion mass is reduced toward its physical value, the energies of the excited states decrease, as the lowest-lying excited state is typically a nucleon–pion ($N\pi$) in a relative P-wave. At the same time, the energy scale that governs the exponential degradation of the signal also grows. The former issue means calculations must be performed at larger Euclidean times to suppress the slowly decaying excited states, and the latter issue means we need exponentially more statistics to obtain a fixed relative uncertainty at a given Euclidean time.

The most common method of constructing three-point correlation functions follows a strategy similar to the two-point correlation functions, beginning with spatially local sources. A nucleon three-point function with current j_Γ is constructed with interpolating operators $N(t_{\text{sep}},\mathbf{x})$ and $N^\dagger(0,\mathbf{0})$,

$$\begin{aligned} C_\Gamma(t_{\text{sep}},\tau) &= \sum_{\mathbf{x},\mathbf{y}} e^{-i\mathbf{p}\cdot\mathbf{x} + i\mathbf{q}\cdot\mathbf{y}} \langle\Omega|N(t_{\text{sep}},\mathbf{x}) j_\Gamma(\tau,\mathbf{y}) N^\dagger(0,\mathbf{0})|\Omega\rangle \\ &= \sum_{\mathbf{x},\mathbf{y}} e^{-i\mathbf{p}\cdot\mathbf{x} + i\mathbf{q}\cdot\mathbf{y}} e^{-E_n(t_{\text{sep}}-\tau)} e^{-E_m \tau} \langle\Omega|N(0,\mathbf{x})|n\rangle\langle n|j_\Gamma(0,\mathbf{y})|m\rangle\langle m|N^\dagger(0,\mathbf{0})|\Omega\rangle \\ &= \sum_{n,m} z_n(\mathbf{p}) z_m^\dagger(\mathbf{p}-\mathbf{q}) e^{-E_n(t_{\text{sep}}-\tau)} e^{-E_m \tau} g^\Gamma_{n,m}(\mathbf{q}), \end{aligned} \tag{12.}$$

where $g^\Gamma_{n,m}$ are the matrix elements of interest, and in principle, all other quantities can be determined from two-point functions, a point we return to below. Often, the sink is projected to zero momentum, $\mathbf{p} = 0$, and momentum conservation selects an incoming state with momentum $-\mathbf{q}$. A typical calculation is performed with a sequential propagator (84) whose source is obtained by taking forward propagators from the origin and contracting the spin and color indices for all but one quark operator. In the case of the nucleon three-point correlation function, the sequential propagator could originate either from the current insertion or from the sink.[5]

j_Γ: quark bilinear currents of Dirac structure Γ and unspecified flavor structure $\bar{q}\,\Gamma\,q$

$g^\Gamma_{n,m}$: hadronic matrix elements of interest from state m to n with implicit momentum and energy dependence, $\langle n|j_\Gamma|m\rangle$

t_{sep}: the time separation between the sink and source

[5]There are alternative methods for computing nucleon structure known as the one-end trick (85–87) and a variant of the Feynman-Hellmann theorem (88), but these are not in wide use.

The most significant challenge for determining the nucleon matrix elements and subsequent form factors is dealing with the excited-state contamination, an issue that is compounded by the degrading S/N. If the nucleon two-point function is becoming saturated by the ground state at $t \approx 1$ fm, ideally three-point functions would use values of $t_{\text{sep}} \gtrsim 2$ fm. However, the S/N ratio of the three-point functions decays more rapidly than the two-point functions. In practice, a few values of t_{sep} in the range $0.8 \lesssim t_{\text{sep}} \lesssim 1.5$ fm are used, and a fit to the time dependence is used to isolate the ground-state matrix elements. Fits that allow for just one excited state require three values of t_{sep} to avoid being overconstrained. Most results have been generated with three or fewer values of t_{sep}. Reference 25 used many values of t_{sep} to determine g_{A}, and a few other groups have begun advocating the use of many values of t_{sep}, including small values, to improve control over the excited-state contamination (38, 89, 90). Reference 90 used 13 values of t_{sep}, which allowed for a systematic study of the uncertainty associated with the truncation of t_{sep} and a fit to a five-state model.

At nonzero momentum, the trade-off between excited states and S/N becomes more problematic. While the energy associated with the signal grows with the momentum, the energy scale associated with the noise is independent of the momentum. Their difference, which is the energy scale that governs the decay of the S/N, therefore grows with increasing momentum. For values of $Q \gtrsim 2$ GeV, the noise becomes unmanageable unless one uses a smearing profile that couples more strongly to boosted nucleons (91). Parity is also no longer a good quantum number for boosted nucleons, and so the matrix elements couple to both even and odd parity states. Such contamination can be handled through a variational method that incorporates even and odd parity nucleons (92–94).

Recent results have uncovered some additional aspects of excited-state contamination, summarized below.

- Nucleon two-point functions constructed as in Equation 8 are insufficient to reliably determine any of the excited states. Different choices of t_{min} and different reasonable priors in a Bayesian analysis support excited states that differ by several sigma, also resulting in sensitivity of the ground-state spectrum (36, 90) and matrix elements (32, 95).
- In contrast, the curvature in the three-point functions associated with the current insertion time provides extra constraints that make the determination of the spectrum stable and robust while varying t_{min}, the number of excited states, the excited-state model, and the excited-state priors (90). While it is encouraging that the spectrum and matrix elements become stable, such an analysis offers no insight into the nature of the excited states. For example, with typical values of $m_\pi L \approx 4$, the P-wave $N(\mathbf{p})\pi(-\mathbf{p})$ excited-state energy is essentially the same as the nucleon-and-two-pions ($N\pi\pi$) threshold state.
- Many groups determine the spectrum and overlap factors from fits to the two-point functions, and then pass these results into the three-point function analysis without allowing the values to adjust to the global minimum. Such a choice can lead either to an overestimate of the uncertainty of the three-point functions (if one uses the variability of the spectrum mentioned above) or to a biased extraction of the ground-state matrix elements (if one uses the "wrong" value of the spectrum). Given the computational setup described above, the robust choice is to perform a global analysis of the two- and three-point functions simultaneously.
- For zero-momentum transfer, where the spectra of the in and out states have the same value, the use of analysis techniques such as the summation method (96) or a variant of the Feynman-Hellman method (97, 98) can significantly suppress the excited states (90, 99). For nonzero momentum transfer, only the Breit frame, where the momenta of the in and out states are equal and opposite, is amenable to this alternative method (100).

- The excited-state contamination is particularly relevant for the PCAC relation, which we discuss in more detail in Section 3.3.

GGT: generalized Goldberger-Treiman

PPD: pion pole dominance

3.3. Role of Partially Conserved Axial Current in LQCD Results of $F_A(Q^2)$

Given the challenges in identifying all the sources of systematic uncertainty in the calculation of g_A, particularly the excited-state contamination, it is prudent to perform cross checks of observables that test for consistency of results. The validity of the PCAC relation,

$$\partial^\mu A^a_\mu(x) = 2m_q P^a(x), \tag{13.}$$

provides a complex consistency check at nonzero Q^2. Here, A^a_μ and P^a are the axial and pseudoscalar currents, respectively, and m_q is the light quark mass. The PCAC relation is an exact symmetry in the continuum limit. When applied to the axial current matrix element of the nucleon, it yields the Goldberger-Treiman relation, which is usually expressed in the $Q^2 \approx m_\pi^2$ region. For arbitrary Q^2, it is sometimes referred to as the generalized Goldberger-Treiman (GGT) relation,

$$2m_N F_A(Q^2) - \frac{Q^2}{2m_N}\widetilde{F}_P(Q^2) = 2m_q F_P(Q^2), \tag{14.}$$

which provides orthogonal checks of individual matrix elements for the axial and pseudoscalar currents. The axial, induced pseudoscalar, and pseudoscalar form factors of the nucleon (F_A, $\widetilde{F}_P$, and F_P, respectively) appear in this expression, and m_N is the nucleon mass. The pion pole dominance (PPD) ansatz, which is only approximate, even in the continuum limit,

$$\widetilde{F}_P^{PPD}(Q^2) = \frac{4m_N^2}{Q^2 + m_\pi^2} F_A(Q^2), \tag{15.}$$

is obtained by carefully considering the leading asymptotic behavior of the form factors in the double limit $Q^2 \to 0$ and $m_q \to 0$ (101).

Initial calculations targeting the axial form factor verified the PCAC relation for the full correlation functions but found significant *apparent* violations of GGT (43, 102, 103). The resolution of this apparent violation is now informed by baryon χPT, which suggests that chiral and excited-state corrections to the spatial axial, temporal axial, and induced pseudoscalar are functionally different and not properly removed. The axial form factor contributions are largely dominated by loop-level $N\pi$ excited states with a highly suppressed tree-level correction. The correction to the axial form factor is nearly independent of Q^2. On the other hand, corrections to the induced pseudoscalar form factor are driven by the tree-level correction and have a strong Q^2 dependence (104), with the largest correction at low Q^2. The $N\pi$ loop contribution in the induced pseudoscalar is highly suppressed by an approximate cancellation. The contamination to the pseudoscalar current is redundant with the chiral corrections to the axial and induced pseudoscalar form factors and can be obtained by application of the PCAC relation.

Scrutiny of the LQCD data has demonstrated many of the features predicted by χPT. $N\pi$ states were initially expected to be negligible because of a volume suppression of the state overlap, which makes them invisible to the two-point functions (105). However, the three-point axial matrix element can enhance these contributions relative to the ground-state nucleon matrix element, which is enough to overcome the volume suppression. The main excited states that contaminate the temporal axial form factor matrix elements were shown to be driven by two specific $N\pi$ states, characterized by a transition of the nucleon state to an $N\pi$ excited state through the axial current or vice versa (32). In the language of χPT, these states contribute to tree-level $N\pi$ graphs with fixed relative momenta (104). In contrast to the temporal axial insertion, the spatial axial insertion

is expected to be more strongly affected by a tower of loop-level $N\pi$ corrections (104). Taking into account these observations, analyses that fix the spectrum using the two-point functions alone will often miss the important $N\pi$ contamination to the axial matrix element (32, 90).

Nucleon matrix elements of the temporal axial current have the largest visible excited-state contamination (32, 37), which can be at least qualitatively understood with χPT (104). This has led to new analysis strategies that more carefully deal with the $N\pi$ excited state with pion pole contributions and additionally use the temporal axial current correlator to determine excited states. These new strategies yield minimal violations of PCAC and an improved understanding of excited-state contamination on matrix elements sensitive to $F_A(Q^2)$ or $\tilde{F}_P(Q^2)$. Previously, these matrix elements exhibited deviations as large as 40% from the PPD or GGT relations at low Q^2, where they were expected to work best (102, 106).

Although these results are encouraging, they must be reproduced by several independent LQCD calculations for validation. At the time of writing, not all of the results are free from imposed theoretical expectations. To achieve a more stringent validation, the calculations generally would have to be performed where the correlation functions are saturated by the ground state. This could be accomplished by taking the correlation function at large Euclidean times, but the noise is exponentially larger. Given the extreme cost of using such a strategy, a better alternative would be to implement a variational method that allows for the use of multihadron operators that can explicitly remove the $N\pi$ excited states through a diagonalization of the correlation functions (107). We return to this point in Section 5.

3.4. Survey of LQCD Results of $F_A(Q^2)$

The main deliverables from LQCD calculations of the axial form factor are the axial and induced pseudoscalar form factors taken in the continuum, infinite volume, and physical pion mass limits, complete with a set of parameterization coefficients and a covariance matrix. Though the axial coupling and radius are useful for connecting with low-energy applications, such as electro pion production and neutron decay, the needs of neutrino physics in the few-GeV energy range depend on the full momentum transfer dependence of the form factor. Despite the agreement between LQCD and experiment for the axial radius, LQCD predicts an axial form factor that falls off more slowly as a function of Q^2 compared with experiment (see **Figure 3**). If the axial radius were the only parameter determining the form factor Q^2 dependence, then these two observations would be incompatible.

Though the form factor shape, especially when allowed to explore its full uncertainty, is decidedly not a dipole, the central value curve determined from experiment appears to be dipole-like. Restricting to dipole shape only, agreement with the axial radius at $Q^2 = 0$ would mean the axial form factor should agree over the entire relevant Q^2 range, a statement that is not supported by the LQCD data. There is no reason to expect nature to prefer a dipole-like parameterization; the experimental preference toward a dipole-like parameterization is based on a few data sets from the 1970s and 1980s (11, 13, 14) with $O(10^3)$ events at most, on deuterium targets with nuclear corrections that are likely underestimated (18). In addition, the dipole parameterization violates unitarity constraints imposed by QCD (108), and although it has the expected asymptotic behavior at high Q^2, this occurs for a regime well outside of the kinematic range probed by neutrino scattering experiments.

Figure 3 shows the status of existing calculations of the nucleon axial form factor from LQCD compared with the axial form factor obtained from neutrino scattering with deuterium in Reference 18. The RQCD (37) and NME (36) Collaborations have the most mature analyses with several ensembles that probe a range of systematic effects. These computations each have

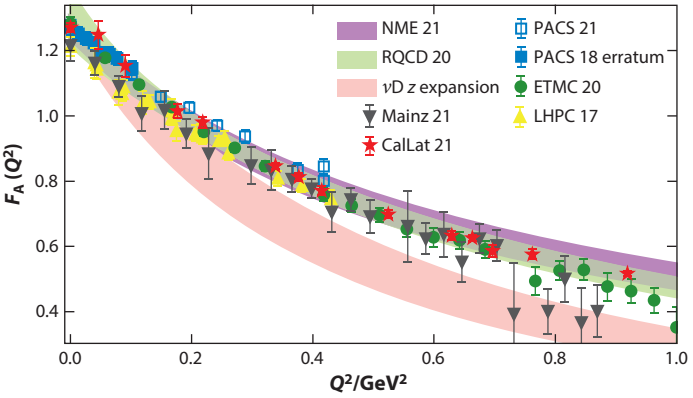

Figure 3

Published results (34, 36, 37, 39, 42, 43, 109–111) for the axial form factor at the physical pion mass obtained from LQCD compared with the deuterium extraction from Reference 18. Results taken from only a single ensemble are plotted as scatter points. These single-ensemble results will have small but unknown corrections due to chiral, continuum, and finite-volume systematic shifts. The NME (36) and RQCD (37) results were both obtained from fits to several ensembles. The RQCD Collaboration performed the full chiral-continuum and finite-volume extrapolations to the data, fitting to each of the form factors independently for each ensemble but providing the constraint that the form factors must satisfy the GGT relation in the continuum. The NME Collaboration also performed a chiral-continuum and finite-volume extrapolation on their data, but their results are based on a fit to their five largest-volume ensembles, neglecting effects from lattice spacing, finite volume, and pion mass. The plotted NME result was obtained by inflating the uncertainty on g_A and b_0 in equation 55 of Reference 36 by a factor of three to account for possible variation due to lattice spacing and quark mass. Abbreviations: CCQE, charged-current quasielastic; GGT, generalized Goldberger-Treiman; LQCD, lattice quantum chromodynamics.

their own methods for addressing the excited-state contamination discussed in Section 3.3, which successfully restore the GGT relation. The RQCD method modifies the parameterization used to fit the correlation function to better constrain the expected shape of excited-state contamination from the $N\pi$ states based on expectations from χPT (104). The NME method tests a variety of Bayesian fits to constrain the excited-state contributions, where the preferred fit enforces a tight prior on the $N\pi$ state at the energy expected from a naive dispersion relation. Because these two results are based on several ensembles, their fits are parameterized and plotted in **Figure 3** as bands rather than as scatter points to distinguish them from estimates on single ensembles.

The ETMC (34), LHPC (109), PACS (42, 43, 110), and CalLat (111) results have just a few ensembles, so in **Figure 3** scatter points obtained from fitting are shown rather than the form factor parameterization to distinguish them from extrapolated results. Though these results are expected to be close to the physical point results, they will have unquantified systematic shifts. The ETMC results have three ensembles, two of which have only two flavors of sea quarks and will be subject to systematics from neglecting sea effects from strange quarks. The form factor data from the remaining ETMC ensemble, a physical pion mass ensemble with four flavors of sea quarks (up, down, strange, and charm), is shown in **Figure 3**. The PACS results are on two different ensembles with physical pion mass, with volumes of $(5.5\text{ fm})^3$ and $(10.8\text{ fm})^3$. The Mainz Collaboration has an ongoing calculation in proceedings on 12 ensembles, including an ensemble at the physical pion mass and a chiral-continuum and infinite-volume extrapolation (39). The results from a two-state fit to their physical pion mass ensemble are plotted with the other results. The CalLat data will be described in more detail in Section 3.4.2.

Chiral-continuum: a simultaneous extrapolation in the pion (quark) mass and the continuum limit

The published results shown in **Figure 3** use different lattice actions for the simulations. The RQCD (37), Mainz (39), and PACS (42, 43, 110) Collaborations use nonperturbatively O(a) improved clover-Wilson fermions for the action and current (the PACS Collaboration notes that the improvement coefficient for the current is consistent with zero, so they do not improve it). The NME (36) and LHPC (109) Collaborations use tree-level (perturbative) O(a) improved clover-Wilson fermions for the action and no improvement for the current. The ETMC (34) Collaboration uses twisted mass fermions [that are automatically O(a) improved] with a clover term, and the CalLat (111) Collaboration uses a mixed-action setup with Möbius DWF on highly improved staggered quark (HISQ) (112) gauge configurations [with leading scaling violations of O(a^2)]. The general agreement between calculations with different actions tests the universality of fermion actions. No obvious tensions are seen, leading to the conclusion that there are no significant scaling violations in the data due to nonzero lattice spacing. The restriction to finite volume has also been probed to some extent by the PACS results, again with no obvious deviations from the results of other collaborations.

low-energy constant (LEC): the coefficient of a hadronic effective field theory operator

The excellent agreement of the axial form factor data and parameterizations for all of the LQCD simulations provides credibility for the claims made by the lattice collaborations, in particular the slow falloff with Q^2. Despite the apparent violations of GGT in the low-Q^2 region, the high-Q^2 region seems to be in better control and less sensitive to the same excited-state contamination. The high-Q^2 agreement is reflected by the restoration of the GGT relation at large Q^2, which is generally the case even for computations that have difficulty satisfying the GGT relation at low Q^2. These claims could be modified by systematic effects that are common to all of the calculations, and excited-state contaminations from $N\pi$ states in the axial form factor remain as a dominant concern. While estimates of excited states using methods that are currently employed by lattice calculations have helped to clarify the situation, modern calculations with $N\pi$-like interpolating operators are needed to definitively quantify the excited-state contaminations over all Q^2. If a dedicated calculation can demonstrate that the excited states are controlled well by the methods presently in use, then worries about the contamination should be more or less resolved.

Another concern is that the magnitude of Q^2 may adversely affect the convergence of the chiral expansion at large Q^2, limiting the ability to extrapolate LQCD results to the physical point. Even for low and moderate values of momentum transfer, a large expansion order would be needed to constrain the form factor dependence on the relevant low-energy constants (LECs), limiting the predictability of the theory. There is some hope that expanding in terms of the z expansion parameter may alleviate some of these concerns by building in correlations between low and high orders of Q^2 that are expected from analyticity. This is discussed in Section 3.5, where we analyze the relationship between Q^2 and z in more detail.

3.4.1. Additional results. In addition to the aforementioned published results, a handful of recent preliminary results deserve mention. The LHPC (109) and PACS (110) Collaborations have explored methods for directly computing the form factor values and slopes directly at $Q^2 = 0$, which offer alternative ways of constraining the form factor shape that could be used to complement traditional methods. The Fermilab Lattice and MILC Collaborations (66, 113, 114) also have an ongoing computation of the axial form factor using a unitary HISQ-on-HISQ setup, for which a preliminary computation of the axial coupling on a single unphysical ensemble exists. Because of the choice of action, this computation has more nucleon "tastes" than other efforts, which is more computationally affordable at the cost of a more challenging analysis.

3.4.2. Description of CalLat data. Since the preliminary CalLat results (111) for the axial form factor are used in Section 4, more discussion about these results is warranted. The CalLat

data were collected on a single ensemble generated by the MILC Collaboration (112) with a lattice spacing $a \approx 0.12$ fm and $m_\pi \approx 130$ MeV. Two-point correlation functions were computed with conjugate source and sink interpolating operators to produce a positive–definite correlation function. The same source and sink operators were used for the three-point functions as well as a local insertion of the $\mathcal{A}_z$ axial current. Up to 10 source–sink separation times were used in the range $t/a \in \{3, \ldots, 12\}$.

The setup used in this analysis fixed $\boldsymbol{q}$ at the current and projected the sink to zero momentum, allowing the source momentum to be fixed by momentum conservation. The momentum $\boldsymbol{q}$ at the insertion was chosen to have $q_z = 0$, which explicitly zeros out all of the contribution to the correlator from the induced pseudoscalar. Momenta up to $|q_{x,y}| \leq 4\sqrt{2} \cdot (2\pi/L)$ were explored, which corresponds to momentum transfers up to around 1 GeV. The ground-state axial matrix element is then proportional to the axial form factor, up to a known kinematic factor. The correlator data were fitted using a parameterization that allows for three states at each momentum.

Once the axial matrix elements were obtained, the form factor data were fitted to a 5 + 4-parameter z expansion, including 4 parameters to enforce sum rules that regulate the large-Q^2 behavior:

$$\left(\frac{\partial}{\partial z}\right)^n \sum_{k=0}^{k_{\max}+4} a_k z^k \Big|_{z=1} = 0; \; n \in \{0, 1, 2, 3\}. \tag{16.}$$

A prior was given to each of the z expansion coefficients of the following form:

$$\text{prior}\left[\frac{a_k}{|a_0|}\right] = 0 \pm \min\left[5, \frac{25}{k}\right]. \tag{17.}$$

No attempt was made to correct for systematics due to lattice spacing, the pion mass mistuning, or the restriction to finite volume, and the uncertainties are statistical only.

The axial form factor coefficients obtained from this procedure (omitting the sum rule coefficients) are as follows:

$$a_k = \{0.914(10), -1.931(54), -0.63(30), 4.4(1.7), -2.2(3.6)\}; \; k \in \{0, 1, 2, 3, 4\}, \tag{18.}$$

which are used in Section 4 without considering their uncertainties.

3.5. Combining the z Expansion with the Continuum and Chiral Extrapolations

Consider an expansion of the form factor as a power series in Q^2 with coefficients that capture the pion mass, lattice spacing, and lattice volume dependence:

$$F(Q^2) = \sum_{k=0} f_k(m_\pi, a, L) Q^{2k}. \tag{19.}$$

This expression will be valid for arbitrarily small values of m_π, Q, and a and for sufficiently large values of L. However, it is not valid for large values of Q; perturbative QCD predicts that the form factor should scale as Q^{-4} in the asymptotically large Q^2 regime. For sufficiently small values of m_π and Q (and large L), χPT (115–117) provides a model-independent parameterization of the coefficients, f_k. χPT can be extended to incorporate the lattice spacing corrections as well (118).

However, the LQCD calculations of the form factors are typically carried out up to $Q^2 \approx 1$–3 GeV^2, well outside the range of validity of χPT,[6] complicating a combined extrapolation in the

[6]The range of validity of χPT in the pion mass seems to be at best $m_\pi \lesssim 300$ MeV (119, 120), and there are some indications that the convergence is troubled at the physical pion mass (45, 121). A similar upper limit in Q is likely.

various variables of interest. For quantities such as the spectrum and nucleon axial, scalar, and tensor couplings, results at heavier pion masses can help improve the overall precision of the final result provided the extrapolation to the physical pion mass is under control. For the form factors, there is still an issue related to the continuum extrapolation even when using only ensembles with physical pion masses and large volumes with negligible volume corrections. The reason is that the spatial extent, L, is given by the lattice spacing times the number of spatial sites, N. In practice, given the nontrivial relation between the lattice spacing a, a derived quantity, and the bare gauge coupling that is an input parameter of the calculation, it is not possible to change a in such a way that $L = Na$ is constant. The allowed quantized momentum for the nucleon and currents will therefore change as the lattice spacing is changed, which means the value of the four-momentum transfer Q will not be the same from one physical pion mass ensemble to the next. Consequently, the continuum extrapolation, which is straightforward in principle, is complicated in practice, minimally requiring a combined extrapolation in Q and a. Is it possible to perform a combined extrapolation/interpolation analysis over the full range of individual Q while also taking the continuum and physical pion mass limits?

The z expansion takes advantage of the analytic structure of QCD by performing a conformal mapping to obtain a new small expansion parameter. This technique has been used for decades in meson flavor physics (122) and is a standard feature in modern LQCD calculations of meson form factors that constrain CKM matrix elements. The z expansion takes the four-momentum transfer squared Q^2 to a small expansion parameter z, using the following relation:

$$z(t = -Q^2; t_0, t_c) = \frac{\sqrt{t_c - t} - \sqrt{t_c - t_0}}{\sqrt{t_c - t} + \sqrt{t_c - t_0}}. \quad 20.$$

Both t_0 and t_c are parameters that can be chosen, with some restrictions. t_c cannot be larger than the particle production threshold in the timelike momentum transfer, and t_0 is a parameter (typically negative) that may be chosen to improve the series convergence. Inverting this relation and expanding as a power series in z about $Q^2 = -t_0$ ($z = 0$) yields

$$x \equiv \frac{Q^2 + t_0}{t_c - t_0} = 4 \sum_{k=1}^{\infty} k z^k. \quad 21.$$

Following this procedure, the dimensionful coefficients f_k in Equation 19 are assembled into expressions related to the dimensionless coefficients of the z expansion (which we denote here by b_k to avoid confusion with the lattice spacing a):

$$F[z(Q^2; t_0, t_c)] = \sum_{k=0}^{\infty} b_k z^k. \quad 22.$$

The most recent multiensemble LQCD publications with computations of the axial form factor (36, 37) have treated the z expansion coefficients as the relevant LECs and fitted to these coefficients with a chiral-continuum extrapolation. As discussed above, for sufficiently small m_π, Q, and a, the coefficients f_k have a well-defined expansion that is rooted in χPT and its extension to incorporate discretization. This is possible because there is a rigorous mapping between the quark-level operators in QCD and the higher-order Symanzik expansion with hadronic-level operators in the EFT. For a dynamic quantity, such as the form factor, or the z expansion parameterization of it, it is not guaranteed that the coefficients can be described with simple m_π and a expansions. For pion masses that are sufficiently close to the physical pion mass, and for lattice spacings sufficiently close to the continuum limit, a Taylor expansion about these limits should be adequate to interpolate and extrapolate with controlled uncertainties. For some quantities, such as the proton radius, there are divergent $\ln(m_\pi)$ corrections that arise in the χPT description, which

are observed as rapid pion mass dependence in LQCD calculations (see, e.g., Reference 123). Such corrections as these, or possibly important $a^2\ln(a)$ corrections that arise in lattice perturbation theory (124–126), if relevant, may not be easily or correctly captured by parameterizing the z expansion coefficients as a power series in a and/or m_π. There is the additional subtlety of understanding and incorporating the finite-volume corrections, which are well understood in the regime where χPT is applicable (127), but we will not comment on this in further detail.

We propose a strategy that might improve our systematic understanding of these effects, but it needs to be explored to understand its validity and applicability. In essence, the proposal is to begin with the EFT parameterization of the form factor and perform the conformal mapping to express the z expansion coefficients, b_k, in terms of the f_k coefficients that are derived from χPT and its finite-volume and lattice spacing EFT extensions. Then, one can compare the values of the LECs determined in the z expansion analysis over the entire range of data with an analysis of the form factor in the low-m_π and low-Q^2 region using the χPT expression. One could also explore simultaneous fits with both methods, where one uses higher-order terms in the z expansion, if needed, which could also help quantify corrections that cannot be systematically described with the χPT parameterization.

As a slightly more concrete example, start with the inverse transformation from z back to Q^2, expressed in terms of x, given in Equation 21. The expression for z at small x is

$$(1+x)^{1/2} - 1 = \frac{x}{2} - 4\sum_{k=2}^{\infty} \frac{(2k-3)!}{k!(k-2)!}\left(-\frac{x}{4}\right)^k, \quad z = \frac{1}{x}[(1+x)^{1/2}-1]^2, \tag{23.}$$

which starts at $O(x)$. A general series in Q^2 may therefore be converted to a double expansion in z and $t_c - t_0$ by first converting powers of Q^2 to those of $Q^2 + t_0$ and t_0 using the binomial theorem,

$$Q^{2m} = [(Q^2+t_0) - t_0]^m = (t_c - t_0)^m \sum_{n=0}^{m} \binom{m}{n} x^n \left(\frac{-t_0}{t_c - t_0}\right)^{m-n}, \tag{24.}$$

and then substituting Equation 21 to convert powers of x into powers of z. All dependence on the dimension is absorbed into powers of $t_c - t_0 \approx m_\pi^2$. The relative weight of the expansion parameters may be adjusted by changing the value of t_0, giving some modicum of freedom over the expansion order. If we consider the Q^4 expansion of Equation 19 with a truncation at the leading chiral and discretization corrections, we get

$$\begin{aligned} f_0 &= c_0 + \ell_0 m_\pi^2 + d_0 a^2, \\ f_1 &= c_1 + \ell_1 m_\pi^2 + d_1 a^2, \\ f_2 &= c_2 + \ell_2 m_\pi^2 + d_2 a^2, \end{aligned} \tag{25.}$$

where c_k, ℓ_k, and d_k are χPT expressions, including nonanalytic $\ln(m_\pi)$-type and LEC corrections describing the pion mass and lattice spacing dependence. For the axial form factor, c_0 and c_1 are related to the axial coupling and radius in the chiral limit

$$c_0 = \lim_{m_\pi \to 0} g_A, \qquad c_1 = -\lim_{m_\pi \to 0} \frac{g_A r_A^2}{6}. \tag{26.}$$

Then the z expansion coefficients that appear in Equation 22, expressed in terms of f_k, are

$$\begin{aligned} b_0 &= f_0 + (t_c - t_0)\left(\frac{-t_0}{t_c - t_0}\right) f_1 + (t_c - t_0)^2 \left(\frac{-t_0}{t_c - t_0}\right)^2 f_2 + O[(t_c - t_0)^3], \\ b_1 &= 4(t_c - t_0) f_1 + 8(t_c - t_0)^2 \left(\frac{-t_0}{t_c - t_0}\right) f_2 + O[(t_c - t_0)^3], \\ b_2 &= 8(t_c - t_0) f_1 + 16(t_c - t_0)^2 \left(1 - \frac{t_0}{t_c - t_0}\right) f_2 + O[(t_c - t_0)^3]. \end{aligned} \tag{27.}$$

The leading lattice spacing, pion mass, and finite-volume dependence may be made manifest by substituting their expressions from Equation 25.

4. PHENOMENOLOGICAL IMPACT

Neutrino oscillation experiments measure an event rate, which is the convolution of the flux, cross section, and detector efficiency, as a function of some measurable variable. The incoming neutrino energy is not known event by event, and not all outgoing particles are detectable, so quantities such as the energy transfer or four-momentum transfer cannot be reconstructed. As neutrino oscillation is a neutrino energy–dependent (and distance-dependent) phenomenon, experiments attempt to reconstruct it using the kinematics of particles produced when neutrinos interact in their detectors.

T2K, and other experiments with a relatively low-energy ($\lesssim$1 GeV) beam (4, 128), attempt to reconstruct the neutrino energy using outgoing lepton momentum, p_l, and its angle with respect to the incoming beam direction, θ_l, assuming two-body quasielastic kinematics with the initial nucleon at rest,

$$E_\nu^{\mathrm{rec,QE}}(p_l,\theta_l) = \frac{2m_f\sqrt{p_l^2+m_l^2} - m_l^2 + m_i^2 - m_f^2}{2\left(m_f - \sqrt{p_l^2+m_l^2} + p_l\cos\theta_l\right)}, \qquad 28.$$

where m_l is the mass of the outgoing lepton, m_i is the mass of the initial-state nucleon, and m_f is the mass of the final-state nucleon. As this variable assumes quasielastic kinematics, it is applied to a signal sample of CC0π events.[7] Events that are not true CCQE events also contribute to the CC0π signal, such as charged-current interaction with two nucleons (CC-2p2h) or charged-current resonant pion production (CC-RES) with no visible final-state pion. The two-body approximation in Equation 28 is a poor approximation of the true neutrino energy, E_ν^{true}, in these cases. Understanding the relative fraction of the different interaction channels is therefore a critical issue for experiments that use Equation 28.

Figure 4 shows the ν_μ-H_2O CC0π event rates expected at the T2K experiment's near and far detectors for a fixed exposure, shown as a function of $E_\nu^{\mathrm{rec,QE}}(p_l,\theta_l)$, with and without modifications to the axial form factor. The nominal GENIEv3 10a_02_11a model (132, 133) uses a dipole axial form factor with mass parameter $M_A = 0.941$ GeV obtained through a fit to bubble-chamber data (134). The alternative model shown differs only in the use of the z expansion model for the axial form factor, with parameters tuned to the LQCD results from the CalLat Collaboration described in Section 3.4.2. One obvious observation to be made from **Figure 4** is that the CCQE events, for which the axial form factor is relevant, make up the majority of the T2K CC0π sample in both the oscillated and unoscillated fluxes. The tuned LQCD values have a significant effect on the total expected event rate in both cases, on the order of 20%.

Also clear from **Figure 4** is that the change in both the total and CCQE-contributed event rates is not purely a normalization change but instead depends on neutrino energy and is different for the near and far detectors. In the T2K oscillation analysis, the near-detector data are used to constrain the cross-section model and reduce the uncertainty at the far detector and on the measured oscillation parameters. If there is insufficient freedom in the cross-section model to account for this change to the CCQE model, other parts of the model may well be distorted to ensure good agreement with the near-detector data. However, this can introduce biases at the far detector, as the different interaction types that contribute to the CC0π samples shown in **Figure 4**

[7]Note that in recent analyses, the T2K experiment has included samples with a single charged pion using a modified version of Equation 28 (129–131).

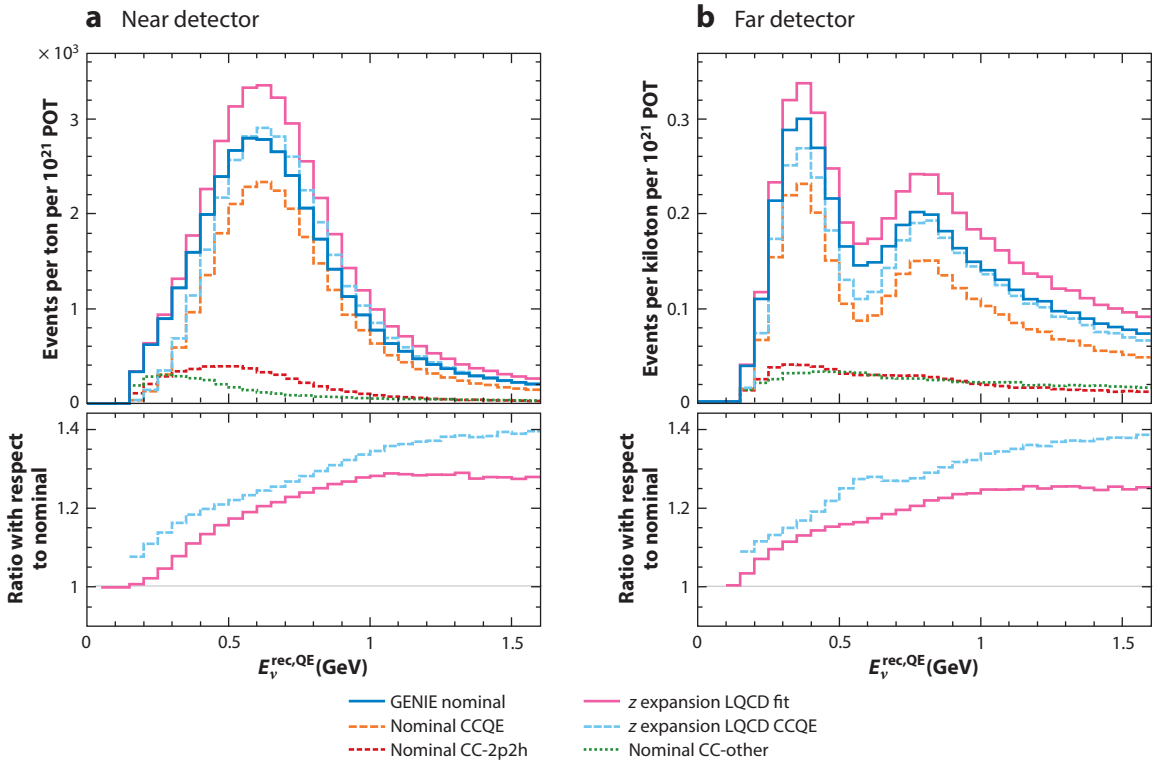

Figure 4

The ν_μ-H_2O CC0π event rates at the T2K experiment's (*a*) near detector and (*b*) far detector sites, shown as functions of $E_\nu^{\mathrm{rec,QE}}$. The GENIE (132, 133) nominal event rate (*blue solid line*) is produced using the GENIEv3 10a_02_11a tune to nucleon data (134) and the T2K flux (135). The CCQE (*orange dashed line*), CC-2p2h (*red short dashed line*), and CC-other (*green dotted line*) contributions are shown (here, CC-other refers to all events that are not CCQE or CC-2p2h). The oscillated flux is calculated using the best-fit NuFit5.0 oscillation parameters in normal ordering (1, 136). Additionally, an alternative GENIE model is shown, where the only change is to use the *z* expansion model of the axial form factor, with parameters tuned to LQCD results from the CalLat Collaboration, as described in Section 3.4.2. The ratio of the modified to nominal GENIE models is shown in the bottom part of each panel. Abbreviations: CC, charged current; CCQE, charged-current quasielastic; CC-2p2h, charged-current interaction with two nucleons; LQCD, lattice quantum chromodynamics.

have very different E_ν^{true}-$E_\nu^{\mathrm{rec,QE}}$ relationships. So if other components of the model are distorted to fit the unoscillated near-detector event rate, that same effective change is not in general expected to extrapolate to the far-detector spectrum correctly.

Experiments with higher neutrino beam energies typically do not limit their analyses to CC0π events or use Equation 28 to reconstruct the neutrino energy. Instead, they use all charged-current events (CC-inclusive) and reconstruct the neutrino energy through a combination of particle identification and tracking together with calorimetry. For an ideal detector with no tracking threshold on protons, charged pions, or electromagnetic activity, this can be expressed as follows:

$$E_\nu^{\mathrm{rec,had}} = E_l + \Sigma_p E_{\mathrm{kin}} + \Sigma_{\pi^\pm,\pi^0,\gamma} E_{\mathrm{total}}, \qquad 29.$$

where E_l is the energy of the outgoing charged lepton, and E_{kin} and E_{total} indicate the kinetic and total energies of individual outgoing hadrons. The E_ν^{true}-$E_\nu^{\mathrm{rec,had}}$ smearing in this idealized case is due to missing kinetic energy lost to neutrons and initial-state nuclear effects (e.g., nucleons are not at rest inside the nucleus). Real detectors have tracking thresholds below which charged

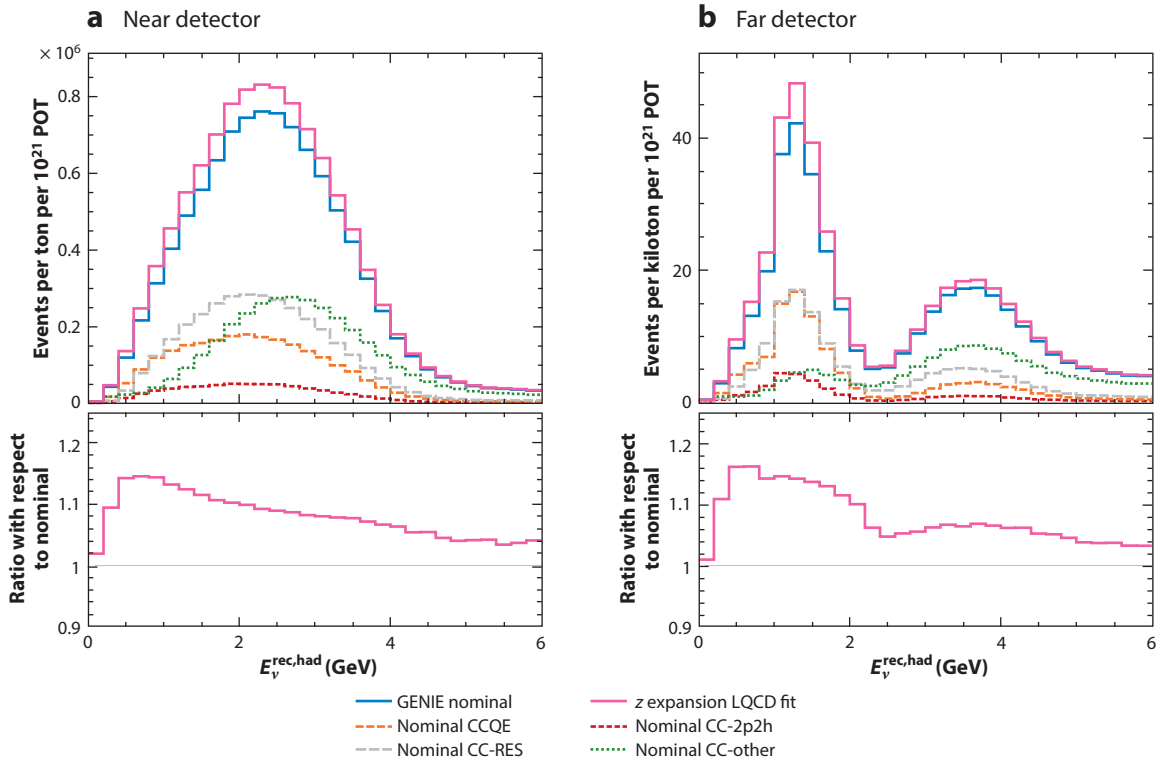

Figure 5

The ν_μ-^{40}Ar CC-inclusive event rates at the DUNE experiment's (*a*) near detector and (*b*) far detector sites, shown as functions of $E_\nu^{\text{rec,had}}$. The GENIE (132, 133) nominal event rate (*blue solid line*) is produced using the GENIEv3 10a_02_11a tune to nucleon data (134) and the DUNE flux (137). The CCQE (*orange dashed line*), CC-2p2h (*red short dashed line*), CC-RES (*long-dashed gray line*), and CC-other (*green dotted line*) contributions are shown (here, CC-other refers to all events that are not CCQE, CC-2p2h, or CC-RES). The oscillated flux is calculated using the best-fit NuFit5.0 oscillation parameters in normal ordering (1, 136). Additionally, an alternative GENIE model is shown, where the only change is to use the *z* expansion model of the axial form factor, with parameters tuned to LQCD results from the CalLat Collaboration, as described in Section 3.4.2. The ratio of the modified to nominal GENIE models is shown in the bottom part of each panel. Abbreviations: CC, charged current; CCQE, charged-current quasielastic; CC-2p2h, charged-current interaction with two nucleons; CC-RES, charged-current resonant pion production; LQCD, lattice quantum chromodynamics.

particles cannot be reconstructed, resulting in additional smearing due to missing the masses of charged pions, although some energy lost to neutrons may be recovered.

Figure 5 shows the ν_μ-^{40}Ar CC-inclusive event rates at the DUNE experiment's near and far detector sites, shown as functions of $E_\nu^{\text{rec,had}}$, with and without modifications to the axial form factor. At this higher neutrino beam energy (with $E_\nu^{\text{peak}} \approx 2.5$ GeV), CCQE events still make up a sizable (∼30%) fraction of the total events. The modification to the axial form factor based on the LQCD results from the CalLat Collaboration described in Section 3.4.2 results in an approximately 10% enhancement to the total predicted event rate at both the near and far detectors. As in the case with the T2K event rate, the enhancement has a nontrivial neutrino energy dependence. Despite the different neutrino energy reconstruction methods used in the DUNE and T2K experiments, the same arguments about potential bias due to model dependence apply when there are differences in the effect of an out-of-model change between near and far detectors.

The issue of how to assign strength between the CCQE and CC-2p2h channels has been a major focus for neutrino oscillation experiments over the past decade. Data from a large number of experiments have disagreed with model predictions in the CC0π channel at the 10–30% level (2, 7–10). This has prompted development of ad hoc systematic uncertainties and empirical model tunings unique to each experiment, with a tendency to soak up model–data discrepancies into the CC-2p2h channel. These are major contributors to the final uncertainties on key oscillation parameter measurements and projected sensitivities (130, 131, 138–140). It is therefore very significant that the LQCD results shown in **Figures 4** and **5** suggest that an increase in the strength of the CCQE contribution on the order of 20% is necessary.

5. FUTURE IMPROVEMENTS

The most pressing issue that needs to be definitively resolved for the LQCD calculations is whether the excited-state contamination is under complete control for the nucleon (quasi-)elastic form factor calculations. If it is, then the LQCD results imply that the nucleon axial form factor is significantly different from what has been extracted phenomenologically, as indicated in **Figure 3**. However, it is worth observing that LQCD calculations of g_A were systematically low for many years before the issue was finally understood to be related to an underestimation of the systematic uncertainty associated with these excited states.

There are several groups computing these form factors with several different lattice actions and several different approaches to quantifying and removing the excited-state contamination from the ground-state matrix elements. Given the heightened awareness of this issue, it is much less likely that all the LQCD results are polluted by such a contamination than was the case for g_A. The most clear way to definitively resolve the question would be to perform an extremely high-statistics calculation with source–sink separation times of $t_{sep} \approx 2$–3 fm. The extreme numerical cost renders this an unlikely approach. In the longer term, the use of multilevel integration schemes can lead to an exponentially improved stochastic precision (141).

A much more practical solution presently would be to implement a variational calculation using distillation (142) or its stochastic variant (143). There are several advantages to such a calculation. First, these methods enable the use of multihadron creation and annihilation operators that are essential to properly identify both the spectrum and the nature of the state (144, 145), whether it is a P-wave $N\pi$ state, some radial excitation of the nucleon such as the Roper that prominently decays to an $N\pi\pi$ state, or otherwise. Given this information, one can construct linear combinations of these operators that systematically remove the excited states from the correlation function (107), allowing for the use of much earlier Euclidean times in which the stochastic noise is relatively much smaller. Second, these variational methods enable the use of momentum space creation as well as annihilation operators with full control over the spin projection of the source and sink at minimal extra cost. This enables one to construct useful linear combinations of correlation functions that eliminate, for example, the induced pseudoscalar contribution to an axial three-point function, which simplifies the analysis (146). Further, one can exploit the Breit frame in which magnitude of the incoming and outgoing momenta are the same; this opens the door for using the Feynman-Hellmann-like correlation functions, which suppress the excited-state contamination significantly compared with the three-point functions (90). It is encouraging that the first exploratory calculations with such methods have begun (147, 148).

Moving beyond these simplest quantities, higher-energy-transfer processes also play a subdominant role for T2K (and the future Hyper-K) experiments and a major role in the DUNE experiment, which has a higher-energy neutrino flux, as can be seen in **Figures 4** and **5**, respectively. These higher-energy transfers can access other fundamentally different interaction topologies,

such as resonant or nonresonant pion production mechanisms, nuclear responses with correlated nucleon pairs, and scattering off partons within nucleons. In principle, all of these interaction mechanisms are accessible to LQCD, though with varying degrees of difficulty. Given the discrepancy between lattice axial form factor data and experimental constraints, it is not unreasonable to expect that other interaction mechanisms have similar discrepancies between theory and observation. These interaction types are as inaccessible as CCQE with modern νA data; they typically rely on old H_2 and D_2 bubble-chamber data sets with even lower statistics than the historic CCQE data sets discussed above, all of which compounds the problem. Appeals to model assumptions may give some handle for missing quantities but are also subject to unquantifiable systematic effects.

Calculations that access the combined resonant and nonresonant scattering amplitudes are the most similar to those of elastic scattering, where a current induces a transition of the nucleon to a multiparticle final state. The most prominent resonant contribution is from the $N \to \Delta$ transition. However, building up an understanding of the entire resonant region, following the standard LQCD computational strategy, will be an extremely challenging endeavor given the dense spectrum of multiparticle states and, more importantly, the lack of formalism to relate three-particle matrix elements in finite volume to the infinite-volume physics of interest. Alternative strategies that focus on the inclusive $N \to X$ contribution (149–152) or the use of two currents to compute the hadronic tensor (153, 154) are likely to be more fruitful.

Calculations of two-nucleon matrix elements provide key insights about the correlations between nucleons inside a nuclear medium, a vital ingredient for construction of an effective theory of νA interactions. The first efforts have been made to compute two-nucleon matrix elements in response to electroweak currents (155, 156). These calculations will most likely have to be revisited with a variational method as well since it now appears that the use of local two-nucleon creation operators does not correctly reproduce the spectrum (157–160). Future calculations of matrix elements for currents inserted between two-nucleon states could provide direct information about the LEC inputs to EFT descriptions of nuclear physics. While EFTs cannot be used to describe the νA response over the full kinematic range of interest, they can provide a crucial anchor point to constrain nuclear models (see, e.g., 121, 161–163). As a specific example, deuterium corrections from nuclear models were assumed to be strong only at low momentum transfer and energy-independent in the reanalysis of deuterium bubble-chamber data (18) despite the inability of these corrections to account for the theory–data discrepancies. A direct LQCD computation of these effects would isolate the effect, either by definitively attributing the discrepancy to deuterium effects or by implicating the other systematic corrections.

6. CONCLUSIONS

LQCD collaborations are able to produce consistent results for benchmark quantities such as g_A with percent-level systematic uncertainties, which are in excellent agreement with experimental data. These results introduce the exciting possibility of using LQCD calculations to tackle other quantities that are not easily accessible experimentally or for which tensions between measurements or competing models exist. In this review, we have discussed LQCD calculations of nucleon form factors as a function of momentum transfer, which are of particular interest to the few-GeV neutrino experimental program. Here we have focused on the axial form factor, $F_A(Q^2)$, which is of primary importance because current parameterizations are simplistic and rely on a handful of low-statistics νN bubble-chamber measurements. However, notable tensions exist in current parameterizations of the vector form factors too. $F_A(Q^2)$ cannot be cleanly measured with existing experiments that use heavier nuclear targets both for safety reasons and to increase the event rate, so LQCD offers a novel path to this important quantity. We have compared $F_A(Q^2)$ calculations

from a variety of different LQCD collaborations using different approaches and techniques, and we have shown them to be in good agreement with each other but, crucially, in poor agreement with the simple dipole model tuned to the historic νN data that are currently relied upon. Assuming that no systematic effects that would affect all of the LQCD calculations are uncovered, this suggests a significant increase of approximately 20% to the strength of the CCQE scattering channel that dominates the neutrino scattering cross section for $E_\nu \lesssim 1$ GeV.

While it is possible that the lattice community will uncover additional systematic uncertainties in the calculation of the axial form factor, given the current state of understanding in the field, we believe this is unlikely. The consistency of the various incomplete LQCD results at the physical pion mass lends confidence to this assessment, and these results will continue to be refined and substantiated. Given the state of the field and the rapid advances recently made, we anticipate that the systematic uncertainties will be fully understood within a year or two, thus enabling precise determinations of the quasielastic axial form factor and the elastic electric and magnetic form factors. At this point, LQCD will be able to resolve the experimental and phenomenological discrepancies reviewed in Section 2.

We have demonstrated that these results produce a significant change in the predicted neutrino event spectra for the T2K (which has similar considerations to Hyper-K) and DUNE experiments. Determining the impact on oscillation results would require a full analysis performed by each experimental collaboration, but it is clear that LQCD results for $F_A(Q^2)$ may offer valuable insight that can clarify aspects of the complex neutrino interaction modeling problem these experiments face. We also have discussed a number of ways that current calculations can be improved and validated, to increase confidence that the LQCD results are not subject to an uncontrolled systematic uncertainty. Finally, we have discussed a number of other quantities that are important to neutrino oscillation experiments in the few-GeV energy regime and for which LQCD can provide first-principles predictions. These include resonant pion production at higher-energy transfers (of particular interest in the DUNE experiment) and insights into nucleon–nucleon correlations, for which there are no clear experimental prospects. These possibilities would all work to break current degeneracies between νN interactions and various nuclear effects that come into play for present modeling efforts of the νA cross sections.

NOTE ADDED IN PROOF

After this review was completed, the Mainz Collaboration updated their results presented in the Lattice Proceedings (39) with a paper (164) containing a full extrapolation to the physical point (see **Figure 3**).

DISCLOSURE STATEMENT

While the authors' collaboration affiliations do not affect the objectivity of this review, we wish to include them for transparency. A.S.M. and A.W.-L. are both current members of the CalLat Collaboration. A.S.M. is a current member of the Fermilab Lattice and MILC Collaborations. C.W. is a current member of the T2K and DUNE Collaborations. The authors are not aware of any funding or financial holdings that might be perceived as affecting the objectivity of this review.

ACKNOWLEDGMENTS

The work of A.S.M. was supported by the US Department of Energy, Office of Nuclear Physics, under contract DE-SC00046548. The work of A.W.-L. and C.W. was supported by the Director, Office of Science, Office of Basic Energy Sciences, of the US Department of Energy under contract DE-AC02-05CH11231.

LITERATURE CITED

1. Esteban I, et al. *J. High Energy Phys.* 2009:178 (2020)
2. Zyla PA, et al. *PTEP* 2020:083C01 (2020)
3. Abi B, et al. *J. Instrum.* 15:T08008 (2020)
4. Abe K, et al. arXiv:1805.04163 [physics.ins-det] (2018)
5. Formaggio JA, Zeller GP. *Rev. Mod. Phys.* 84:1307 (2012)
6. Alvarez-Ruso L, Hayato Y, Nieves J. *New J. Phys.* 16:075015 (2014)
7. Mosel U. *Annu. Rev. Nucl. Part. Sci.* 66:171 (2016)
8. Katori T, Martini M. *J.Phys. G* 45:013001 (2018)
9. Alvarez-Ruso L, et al. *Prog. Part. Nucl. Phys.* 100:1 (2018)
10. Garvey GT, et al. *Phys. Rep.* 580:1 (2015)
11. Barish S, et al. *Phys. Rev. D* 16:3103 (1977)
12. Fanourakis G, et al. *Phys. Rev. D* 21:562 (1980)
13. Baker N, et al. *Phys. Rev. D* 23:2499 (1981)
14. Kitagaki T, et al. *Phys. Rev. D* 28:436 (1983)
15. Allasia D, et al. *Nucl. Phys. B* 343:285 (1990)
16. Bernard V, Kaiser N, Lee TSH, Meissner UG. *Phys. Rep.* 246:315 (1994)
17. Bernard V, Elouadrhiri L, Meissner UG. *J. Phys. G* 28:R1 (2002)
18. Meyer AS, Betancourt M, Gran R, Hill RJ. *Phys. Rev. D* 93:113015 (2016)
19. Hill RJ, Kammel P, Marciano WJ, Sirlin A. *Rep. Prog. Phys.* 81:096301 (2018)
20. Lu XG, et al. *Phys. Rev. D* 92:051302 (2015)
21. Munteanu L, et al. *Phys. Rev. D* 101:092003 (2020)
22. Hamacher-Baumann P, Lu X, Martín-Albo J. *Phys. Rev. D* 102:033005 (2020)
23. Abed Abud A, et al. *Instruments* 5:31 (2021)
24. Cai T. 2021. *Measurements of nuclear effects and the* $\bar{\nu}_\mu + H \to \mu^+ + n$ *cross section in MINERv A with neutron tagging*. PhD Thesis, Rochester Univ., Rochester, NY
25. Chang CC, et al. *Nature* 558:91 (2018)
26. Bradford R, Bodek A, Budd HS, Arrington J. *Nucl. Phys. B Proc. Suppl.* 159:127 (2006)
27. Borah K, Hill RJ, Lee G, Tomalak O. *Phys. Rev. D* 102:074012 (2020)
28. Dubbers D, Märkisch B. *Annu. Rev. Nucl. Part. Sci.* 71:139 (2021)
29. Aoki Y, et al. arXiv:2111.09849 [hep-lat] (2021)
30. Bär O. *Int. J. Mod. Phys. A* 32:1730011 (2017)
31. Ottnad K. *Eur. Phys. J. A* 57:50 (2021)
32. Jang YC, Gupta R, Yoon B, Bhattacharya T. *Phys. Rev. Lett.* 124:072002 (2020)
33. Gupta R, et al. *Phys. Rev. D* 98:034503 (2018)
34. Alexandrou C, et al. *Phys. Rev. D* 103:034509 (2021)
35. Abramczyk M, et al. *Phys. Rev. D* 101:034510 (2020)
36. Park S, et al. *Phys. Rev. D* 105:054505 (2022)
37. Bali GS, et al. *J. High Energy Phys.* 2005:126 (2020)
38. Hasan N, et al. *Phys. Rev. D* 99:114505 (2019)
39. Djukanovic D, et al. arXiv:2112.00127 [hep-lat] (2021)
40. Harris T, et al. *Phys. Rev. D* 100:034513 (2019)
41. Liang J, et al. *Phys. Rev. D* 98:074505 (2018)
42. Shintani E, et al. *Phys. Rev. D* 99:014510 (2019). Erratum. *Phys. Rev. D* 102:019902 (2020)
43. Ishikawa KI, et al. *Phys. Rev. D* 98:074510 (2018)
44. Berkowitz E, et al. In *SC18: International Conference for High Performance Computing, Networking, Storage and Analysis*, pp. 697–705. Piscataway, NJ: IEEE (2018)
45. Walker-Loud A, et al. *Proc. Sci.* CD2018:020 (2020)
46. Smit J. *Introduction to Quantum Fields on a Lattice: A Robust Mate*. Cambridge, UK: Cambridge Univ. Press (2011)
47. DeGrand T, Detar CE. *Lattice Methods for Quantum Chromodynamics*. Singapore: World Scientific (2006)
48. Gattringer C, Lang CB. *Quantum Chromodynamics on the Lattice*. Berlin: Springer (2010)

49. Duane S, Kennedy AD, Pendleton BJ, Roweth D. *Phys. Lett. B* 195:216 (1987)
50. Clark M, et al. *Comput. Phys. Commun.* 181:1517 (2010)
51. Babich R, et al. In *SC '11: Proceedings of 2011 International Conference for High Performance Computing, Networking, Storage and Analysis*, Article 70. New York: Assoc. Comput. Mach. (2011)
52. Symanzik K. *Nucl. Phys. B* 226:187 (1983)
53. Symanzik K. *Nucl. Phys. B* 226:205 (1983)
54. Wilson KG. *Phys. Rev. D* 10:2445 (1974)
55. Kogut JB, Susskind L. *Phys. Rev. D* 11:395 (1975)
56. Banks T, Susskind L, Kogut JB. *Phys. Rev. D* 13:1043 (1976)
57. Banks T, et al. *Phys. Rev. D* 15:1111 (1977)
58. Susskind L. *Phys. Rev. D* 16:3031 (1977)
59. Sheikholeslami B, Wohlert R. *Nucl. Phys. B* 259:572 (1985)
60. Frezzotti R, Grassi PA, Sint S, Weisz P. *J. High Energy Phys.* 0108:058 (2001)
61. Kaplan DB. *Phys. Lett. B* 288:342 (1992)
62. Shamir Y. *Nucl. Phys. B* 406:90 (1993)
63. Furman V, Shamir Y. *Nucl. Phys. B* 439:54 (1995)
64. Golterman MFL, Smit J. *Nucl. Phys. B* 255:328 (1985)
65. Bailey JA. *Phys. Rev. D* 75:114505 (2007)
66. Lin Y, et al. *Phys. Rev. D* 103:034501 (2021)
67. Luscher M, Sint S, Sommer R, Weisz P. *Nucl. Phys. B* 478:365 (1996)
68. Luscher M, et al. *Nucl. Phys. B* 491:323 (1997)
69. Luscher M, Sint S, Sommer R, Wittig H. *Nucl. Phys. B* 491:344 (1997)
70. Capitani S, Lüscher M, Sommer R, Wittig H. *Nucl. Phys. B* 544:669 (1999). Erratum. *Nucl. Phys. B* 582:762 (2000)
71. Frezzotti R, Rossi GC. *J. High Energy Phys.* 0408:007 (2004)
72. Clark MA, et al. arXiv:1612.07873 [hep-lat] (2016)
73. Boyle PA. arXiv:1402.2585 [hep-lat] (2014)
74. Cohen SD, Brower RC, Clark MA, Osborn JC. *Proc. Sci.* LATTICE2011:030 (2011)
75. Yamaguchi A, Boyle P. *Proc. Sci.* LATTICE2016:374 (2016)
76. Brower RC, Clark MA, Howarth D, Weinberg ES. *Phys. Rev. D* 102:094517 (2020)
77. Boyle P, Yamaguchi A. arXiv:2103.05034 [hep-lat] (2021)
78. Renner DB, et al. *Nucl. Phys. B Proc. Suppl.* 140:255 (2005)
79. Bär O, Rupak G, Shoresh N. *Phys. Rev. D* 67:114505 (2003)
80. Bär O, Bernard C, Rupak G, Shoresh N. *Phys. Rev. D* 72:054502 (2005)
81. Tiburzi BC. *Phys. Rev. D* 72:094501 (2005). Erratum. *Phys. Rev. D* 79:039904 (2009)
82. Chen JW, O'Connell D, Walker-Loud A. *J. High Energy Phys.* 0904:090 (2009)
83. Lepage GP. In *From Actions to Answers: Proceedings of the 1989 Theoretical Advanced Study Institute in Elementary Particle Physics (TASI 1989)*, ed. T Degrand, D Toussaint, pp. 97–120. Singapore: World Scientific (1989)
84. Martinelli G, Sachrajda CT. *Nucl. Phys. B* 316:355 (1989)
85. Foster M, Michael C. *Phys. Rev. D* 59:074503 (1999)
86. McNeile C, Michael C. *Phys. Rev. D* 73:074506 (2006)
87. Alexandrou C, et al. *Eur. Phys. J. C* 74:2692 (2014)
88. Chambers AJ, et al. *Phys. Rev. D* 90:014510 (2014)
89. Alexandrou C, et al. *Phys. Rev. D* 102:054517 (2020)
90. He J, et al. arXiv:2104.05226 [hep-lat] (2021)
91. Bali GS, Lang B, Musch BU, Schäfer A. *Phys. Rev. D* 93:094515 (2016)
92. Stokes FM, et al. *Phys. Rev. D* 92:114506 (2015)
93. Stokes FM, Kamleh W, Leinweber DB. *Phys. Rev. D* 99:074506 (2019)
94. Stokes FM, Kamleh W, Leinweber DB. *Phys. Rev. D* 102:014507 (2020)
95. Gupta R, et al. *Phys. Rev. Lett.* 127:242002 (2021)
96. Maiani L, Martinelli G, Paciello ML, Taglienti B. *Nucl. Phys. B* 293:420 (1987)

97. de Divitiis GM, Petronzio R, Tantalo N. *Phys. Lett. B* 718:589 (2012)
98. Bouchard C, et al. *Phys. Rev. D* 96:014504 (2017)
99. Capitani S, et al. *Phys. Rev. D* 86:074502 (2012)
100. Gambhir AS, et al. *Proc. Sci.* LATTICE2018:126 (2019)
101. Sasaki S, Yamazaki T. *Phys. Rev. D* 78:014510 (2008)
102. Gupta R, et al. *Phys. Rev. D* 96:114503 (2017)
103. Bali GS, et al. *Phys. Lett. B* 789:666 (2019)
104. Bär O. *Phys. Rev. D* 99:054506 (2019)
105. Bär O. *Phys. Rev. D* 94:054505 (2016)
106. Bali GS, et al. *Phys. Rev. D* 91:054501 (2015)
107. Blossier B, et al. *J. High Energy Phys.* 0904:094 (2009)
108. Bhattacharya B, Hill RJ, Paz G. *Phys. Rev. D* 84:073006 (2011)
109. Hasan N, et al. *Phys. Rev. D* 97:034504 (2018)
110. Ishikawa KI, et al. *Phys. Rev. D* 104:074514 (2021)
111. Meyer AS, et al. arXiv:2111.06333 [hep-lat] (2021)
112. Bazavov A, et al. *Phys. Rev. D* 87:054505 (2013)
113. Meyer AS, et al. *Proc. Sci.* LATTICE2016:179 (2016)
114. Lin Y, et al. *Phys. Rev. D* 103:054510 (2021)
115. Gasser J, Leutwyler H. *Nucl. Phys. B* 250:465 (1985)
116. Jenkins EE, Manohar AV. *Phys. Lett. B* 255:558 (1991)
117. Bernard V, Kaiser N, Meissner UG. *Int. J. Mod. Phys. E* 4:193 (1995)
118. Sharpe SR, Singleton RL Jr. *Phys. Rev. D* 58:074501 (1998)
119. Beane SR. *Nucl. Phys. B* 695:192 (2004)
120. Walker-Loud A, et al. *Phys. Rev. D* 79:054502 (2009)
121. Drischler C, et al. *Prog. Part. Nucl. Phys.* 121:103888 (2021)
122. Okubo S. *Phys. Rev. D* 3:2807 (1971)
123. Green JR, et al. *Phys. Rev. D* 90:074507 (2014)
124. Balog J, Niedermayer F, Weisz P. *Phys. Lett. B* 676:188 (2009)
125. Balog J, Niedermayer F, Weisz P. *Nucl. Phys. B* 824:563 (2010)
126. Husung N, Marquard P, Sommer R. *Eur. Phys. J. C* 80:200 (2020)
127. Gasser J, Leutwyler H. *Phys. Lett. B* 184:83 (1987)
128. Aguilar-Arevalo A, et al. *Phys. Rev. D* 103:052002 (2021)
129. Abe K, et al. *Phys. Rev. D* 96:092006 (2017)
130. Abe K, et al. *Nature* 580:339 (2020). Erratum. *Nature* 583:E16 (2020)
131. Abe K, et al. *Phys. Rev. D* 103:112008 (2021)
132. Andreopoulos C, et al. *Nucl. Instrum. Meth. A* 614:87 (2010)
133. Alvarez-Ruso L, et al. *Eur. Phys. J. Special Top.* 230:4449 (2021)
134. Tena-Vidal J, et al. *Phys. Rev. D* 104:072009 (2021)
135. Abe K, et al. *Phys. Rev. D* 87:012001 (2013)
136. Esteban I, et al. Nufit 5.0. *Software Package*. **http://www.nu-fit.org** (2020)
137. Abi B, et al. arXiv:2002.03005 [hep-ex] (2020)
138. Abi B, et al. *Eur. Phys. J. C* 80:978 (2020)
139. Acero MA, et al. arXiv:2108.08219 [hep-ex] (2021)
140. Abud AA, et al. arXiv:2109.01304 [hep-ex] (2021)
141. Cè M, Giusti L, Schaefer S. *Phys. Rev. D* 93:094507 (2016)
142. Peardon M, et al. *Phys. Rev. D* 80:054506 (2009)
143. Morningstar C, et al. *Phys. Rev. D* 83:114505 (2011)
144. Dudek JJ, Edwards RG, Thomas CE. *Phys. Rev. D* 87:034505 (2013). Erratum. *Phys. Rev. D* 90:099902 (2014)
145. Lang CB, Verduci V. *Phys. Rev. D* 87:054502 (2013)
146. Meyer AS. *The nucleon axial form factor and staggered lattice QCD*. PhD Thesis, Univ. Chicago (2017)
147. Egerer C, Richards D, Winter F. *Phys. Rev. D* 99:034506 (2019)

148. Barca L, Bali GS, Collins S. arXiv:2110.11908 [hep-lat] (2021)
149. Hansen MT, Meyer HB, Robaina D. *Phys. Rev. D* 96:094513 (2017)
150. Gambino P, Hashimoto S. *Phys. Rev. Lett.* 125:032001 (2020)
151. Fukaya H, Hashimoto S, Kaneko T, Ohki H. *Phys. Rev. D* 102:114516 (2020)
152. Bruno M, Hansen MT. *J. High Energy Phys.* 2106:43 (2021)
153. Liu KF, Dong SJ. *Phys. Rev. Lett.* 72:1790 (1994)
154. Liang J, et al. *Phys. Rev. D* 101:114503 (2020)
155. Savage MJ, et al. *Phys. Rev. Lett.* 119:062002 (2017)
156. Chang E, et al. *Phys. Rev. Lett.* 120:152002 (2018)
157. Francis A, et al. *Phys. Rev. D* 99:074505 (2019)
158. Hörz B, et al. *Phys. Rev. C* 103:014003 (2021)
159. Green JR, Hanlon AD, Junnarkar PM, Wittig H. *Phys. Rev. Lett.* 127:242003 (2021)
160. Amarasinghe S, et al. arXiv:2108.10835 [hep-lat] (2021)
161. Kronfeld AS, et al. *Eur. Phys. J. A* 55:196 (2019)
162. Tews I, et al. *J. Phys. G* 47:103001 (2020)
163. Davoudi Z, et al. *Phys. Rep.* 900:1 (2021)
164. Djukanovic D, et al. arXiv:2207.03440 [hep-lat] (2022)

Annual Review of Nuclear and Particle Science

Volume 72, 2022

Contents

Errata

An online log of corrections to *Annual Review of Nuclear and Particle Science* articles may be found at http://www.annualreviews.org/errata/nucl